Jun Cai*, Xiaolu Zhang, Kuaishe Wang and Chengpeng Miao

Physics-Based Constitutive Model to Predict Dynamic Recovery Behavior of BFe10-1-2 Cupronickel Alloy during Hot Working

DOI 10.1515/htmp-2015-0094
Received April 13, 2015; accepted November 16, 2015

Abstract: The hot deformation behavior of BFe10-1-2 cupronickel alloy was investigated over wide ranges of deformation temperature and strain rate. The physics-based constitutive model was developed to predict the dynamic recovery (DRV) behavior of BFe10-1-2 cupronickel alloy at elevated temperatures. In order to verify the validity of the developed constitutive equation, the correlation coefficient (R) and average absolute relative error ($AARE$) were introduced to make statistics. The results indicated that the developed constitutive equation lead a good agreement between the calculated and experimental data and can accurately characterize the hot DRV behaviors for the BFe10-1-2 cupronickel alloy.

Keywords: BFe10-1-2 cupronickel alloy, physics-based constitutive model, dynamic recovery, flow stress

Introduction

In the hot working process, the flow behavior of material is complex due to various physical mechanisms occurring such as work hardening (WH), dynamic recovery (DRV) and dynamic recrystallization (DRX), which are affected by the chemical composition of metals and alloys, deformation temperature, deformation degree and strain rate [1]. The constitutive model and/or equation is significant to explore the flow behavior and the optimization of the deformation process of the alloy as it describes the correlation of dynamic material properties with processing parameters [2]. Furthermore, constitutive equation is used as input to the FEM code for simulating the response of materials under the specified deformation conditions [3]. Therefore, the preciseness of the constitutive relation has positive impact on the accuracy of simulation results.

The constitutive relations can be divided into three categories: the phenomenological, physical and artificial neural network (ANN) models. The phenomenological model provides a definition of the flow stress based on empirical observations and consists of some mathematical functions to describe flow behavior of metal materials (WH, strain rate hardening and temperature softening) [4]. Based on the Arrhenius type of equation [5], a phenomenological model has been extensively used to predict the hot deformation behavior of metal materials, such as 42CrMo steel [6], 9Cr-1Mo steel [7], 316 austenitic stainless steel [8], and so on. However, this model is lack of physical background of materials deformation, and just describes flow stress in a simple mathematical form with macroscopic process parameters. Unlike the regression methods, ANN postulates no mathematical model or identifies its parameters. ANN learns from training data and recognizes patterns in a series of input and output values without any prior assumptions about their nature and interrelations [9]. Therefore, it has powerful ability to predict hot deformation behaviors of metal materials across the whole deformation domain and has exactly predicted the flow stress of precipitation-hardening aluminum alloy [10], as-cast TC21 titanium alloy [11], A357 alloy [12], and AZ81 magnesium alloy [13] during hot working. Different from ANN, physics-based constitutive model accounts for physical aspects of the material behaviors such as thermodynamics, thermally activated dislocation movement, and kinetics of slips. Besides, physics-based constitutive model allows for an accurate definition of material behavior under wide ranges of loading conditions by some physical assumptions [4]. Based on the stress–dislocation relation and the kinetics of DRV and DRX, physics-based constitutive relation has been established to describe the flow behavior during the WH, DRV and DRX periods for 55SiMnMo bainite steel [14], D6ac steel [15], Al-Mg Alloy [16], and so on.

***Corresponding author: Jun Cai,** School of Metallurgical Engineering, Xi'an University of Architecture and Technology, Xi'an 710055, China, E-mail: jeffreycai0116@gmail.com
Xiaolu Zhang, Petrochina Company Limited Shaanxi Marketing Company, Xi'an 710004, China
Kuaishe Wang, School of Metallurgical Engineering, Xi'an University of Architecture and Technology, Xi'an 710055, China
Chengpeng Miao, Jinchuan Group Co., Ltd, Jinchang 737104, China

As a kind of a typical Cu-Ni alloy, BFe10-1-2 alloy has been successfully used as cooling-condition material in shipping and seawater desalted industry. The main deformation methods of this alloy include semi-solid casting ingots and hot extrusion, which result in considerable problems, such as long process time, high energy consumption, low product yield and high cost. Therefore, modeling and prediction of the hot deformation behavior of BFe10-1-2 cupronickel alloy is of vital significance for the purpose of improving and accurately controlling the extrusion technology of BFe10-1-2 cupronickel alloy. However, few investigators have focused their research on the physics-based constitutive relation of BFe10-1-2 cupronickel alloy. Therefore, the objective of this investigation is to construct the suitable physics-based constitutive model to characterize the hot DRV behaviors for BFe10-1-2 cupronickel alloy. Toward this end, isothermal hot compression tests were conducted over a wide range of temperature (1,023~1,273 K) and strain rate ($0.001\sim10\ s^{-1}$). The experimental stress–strain data were then employed to derive the physics-based constitutive equation. Finally, the validity of descriptive results obtained from the developed constitutive model was examined over the entire range of temperatures and strain rates.

Experimental procedure

The material investigated in the present study is a commercial as-cast BFe10-1-2 cupronickel alloy, with the following chemical composition (wt%): Ni = 10, Mn = 0.75, Fe = 1.65, Cu = Bal.

Cylindrical specimens with a diameter of 10 mm and a height of 15 mm were machined to carry out compression testing. In order to minimize the friction, the flat ends of the specimens were recessed a depth of 0.1 mm groove to entrap the lubricant. The specimens prior to isothermal compression were heated to the deformation temperature at a rate of 10 °C/s and held for 3 min at the isothermal conditions so as to obtain a uniform deformation temperature. Then isothermal compression tests were performed on a Gleeble-3800 thermo-simulation simulator in the strain rate range of $0.001\sim10\ s^{-1}$ and the temperature range of 1,023~1,273 K. After deformation, the specimens were cooled to room temperature in air. The strain–stress curves were recorded automatically in isothermal compression.

In order to observe the microstructure evolution, the deformed specimens were sectioned parallel to the compression axis, then ground and polished for metallographic examination, and etched with reagent of $FCl + HCl + H_2O$. The microstructure was examined by optical microscopy. In addition, the original microstructure of as received BFe10-1-2 alloy is given in Figure 1.

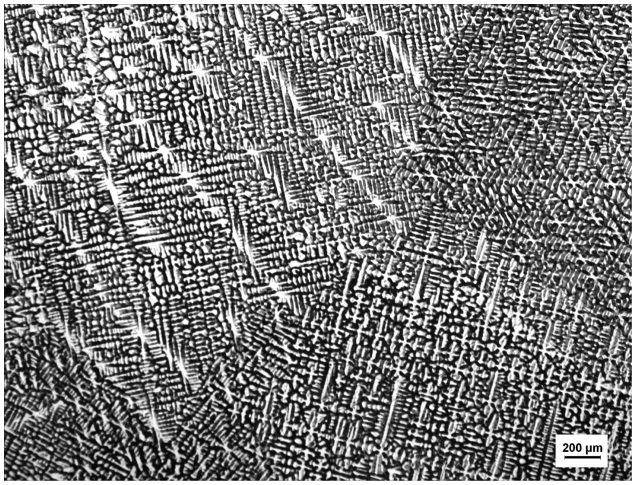

Figure 1: Microstructure of as received BFe10-1-2 alloy.

Results and discussion

Stress–strain characteristics of BFe10-1-2 cupronickel alloy during hot deformation

The true stress–strain curves obtained from the hot compression tests of BFe10-1-2 cupronickel alloy are shown in Figure 2. Although some noise is shown in the curves, it can be seen from figures that the influence of deformation temperature and strain rate on flow stress is significant. From these figures, it can be seen that the flow stress increases with decrease of deformation temperature and increase of strain rate.

The variation of flow stress with the deformation temperature and the strain rate can be expressed quantitatively, and the relationship between deformation temperature, strain rate and dislocation density can be represented as the following formula [1]:

$$\dot{\varepsilon} = \rho_m A \exp\left(-\frac{\Delta G^*}{kT}\right) \tag{1}$$

where $\rho_m = f\rho$ is the mobile dislocation density, f is about 0.1 representing the proportion of the mobile dislocation density in the total dislocation density ρ. A is a materials constant, ΔG^* is the heat activity energy, and k is the Boltzmann constant. Meanwhile, the relationship between

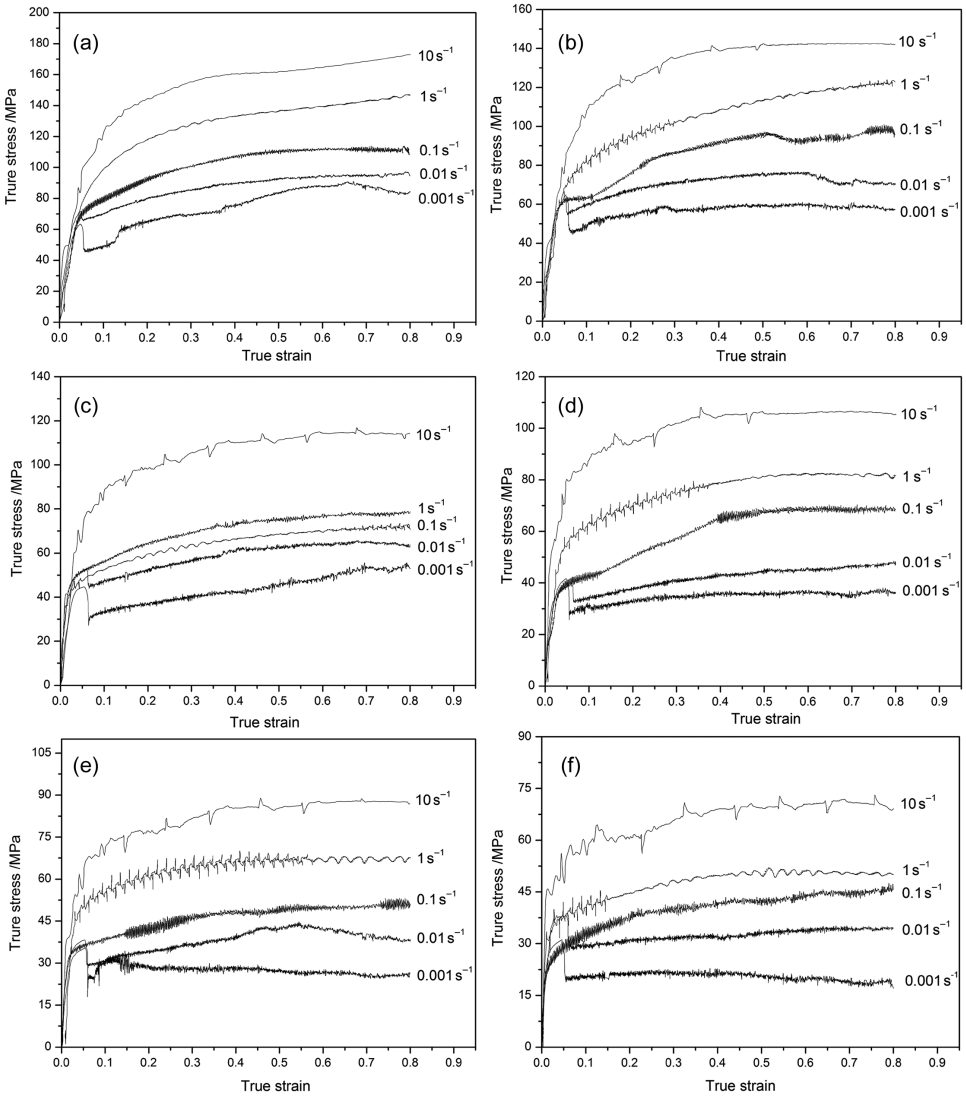

Figure 2: Flow curves of BFe10-1-2 alloy at various strain rates with temperatures of: (a) 1,023 K, (b) 1,073 K, (c) 1,123 K, (d) 1,173 K, (e) 1,223 K, (f) 1,273 K.

the flow stress and the dislocation density can be expressed as:

$$\sigma = \sigma^{\star} + \alpha\mu b\sqrt{\rho} \tag{2}$$

where $\sigma^{\star}$ is the intrinsic strength of materials, b is the Burgers vector, α is the materials constant, and μ is the shear modulus. It can be found from eqs (1) and (2) that the dislocation density decreases with increasing temperatures at a given strain rate, and then the flow stress will increase with the decrease of deformation temperature. Similarly, the dislocation density increases with the increase of strain rates at a given temperature, therefore flow stress will increase with the increase of strain rates.

Meanwhile, the flow stress curves exhibit the DRV characteristics of the material without obvious peak stress. A typical DRV stress–strain curve is given in Figure 3. The flow stress rapidly increases due to WH. When the WH and DRV reach a balance, a saturation flow stress will appear and stay near constant, and the grains continue to elongate with the increase of deformation but the shape and size of subgrains remain unchanged.

Figure 4 illustrates the metallographic microstructure of BFe10-1-2 alloy under various deformation conditions (i. e. 1,023 K, 0.001 s^{-1}; 1,123 K, 0.01 s^{-1}; 1,173 K, 1 s^{-1} and 1,273 K, 10 s^{-1}), where the grains tend to be elongated perpendicular to the compression direction. It can be seen in Figure 2 that flow stresses drop near the strain of 0.6 when strain rate is 0.001 s^{-1} and 0.01 s^{-1} (such as 1,023 and 1,073 K). However, no obvious DRX grains can be detected in Figure 4(a) and (b). Similar phenomenon

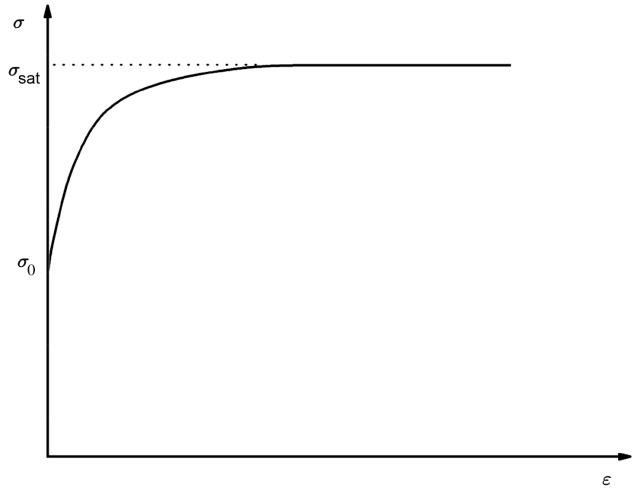

Figure 3: A schematic of true stress–strain curve characteristic of DRV behavior.

was reported by Park [17] in Ti-6Al-4V alloy that the flow softening at slow strain rates was attributed to the occurrence of dynamic spheroidization of the α grains or DRV rather than DRX. Meanwhile, it is difficult for DRV and DRX to occur simultaneously in hot deformation processes because the distortion energy is released by DRV and is accumulated with difficulty to the level for DRX [18]. The dislocation density, distortion energy and recrystallization locations increase with the increasing of strain rate, which leads to the fact that DRX occurs easily at high strain rates [19, 20]. Therefore, the dominant dynamic softening mechanism of BFe10-1-2 alloy is DRV.

Activation energy for hot deformation

The flow stress is mainly influenced by temperature, strain rate and strain during hot working. Zener–Holloman parameter (Z), i. e. temperature modified strain rate, is often used to describe the effects of temperature and strain rate on material deformation behavior:

$$Z = \dot{\varepsilon} \exp\left(\frac{Q}{RT}\right) \tag{3}$$

where $\dot{\varepsilon}$ is the strain rate (s^{-1}), R is the universal gas constant (8.3145 J mol^{-1} K^{-1}), T is the absolute temperature (K), and Q is the activation energy of hot deformation (J/mol). Then a hyperbolic sine equation can be applied predict the flow stress [21]:

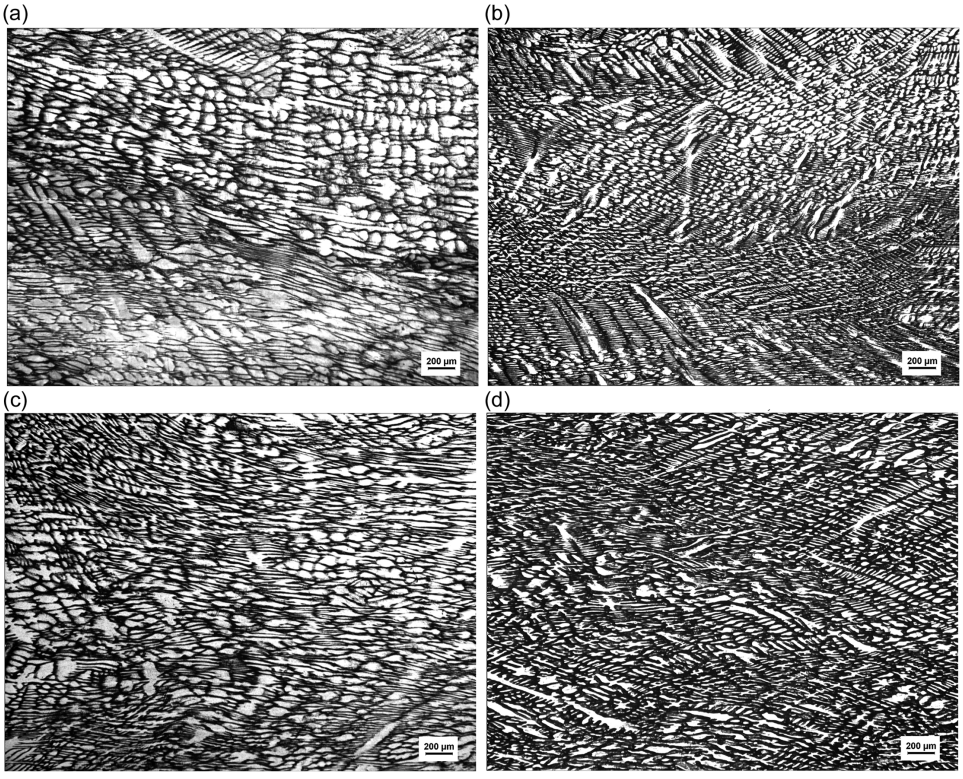

Figure 4: Metallographic microstructure of BFe10-1-2 alloy under the deformation condition of: (a) 1,023 K, 0.001 s^{-1}; (b) 1,123, 0.01 s^{-1}; (c) 1,173, 1 s^{-1}; (d) 1,273, 10 s^{-1}.

$$Z = \dot{\varepsilon}\exp\left(\frac{Q}{RT}\right) = A[\sinh(\alpha\sigma)]^n \tag{4}$$

where A, n and α are material constants, and α can be expressed as:

$$\alpha = \beta/n' \tag{5}$$

where n' and β are the materials constants and can be obtained from following equations:

$$\ln(\sigma) = \frac{1}{n'}\ln(\dot{\varepsilon}) - \frac{1}{n'}\ln(B) \tag{6}$$

$$\sigma = \frac{1}{\beta}\ln(\dot{\varepsilon}) - \frac{1}{\beta}\ln(C) \tag{7}$$

where B and C are the material constants, which are independent of the deformed temperatures. The values of n' and β can be obtained from the slope of the lines in $\ln(\sigma)$–$\ln(\dot{\varepsilon})$ plot and σ–$\ln(\dot{\varepsilon})$ plot, respectively. The relationships of $\ln(\sigma)$–$\ln(\dot{\varepsilon})$ and σ–$\ln(\dot{\varepsilon})$ at the strain of 0.3 are illustrated in Figure 5. The lines are almost parallel indicating that the slope of the lines varies within a very small range. The slight variation in the slope of the lines may be attributed to scattering in the hot compression experimental data. Similar scattering was observed in 42CrMo steel [6], Ti-modified austenitic stainless steel [22], 1Cr12Ni3Mo2VNbN martensitic steel [23], and so on. Possibly, experiment error and physical characteristic lead to the data scattering. For example, a cubic spline function was often used to fit $\ln(\sigma)$–$\ln(\dot{\varepsilon})$ for the purpose of obtaining processing maps [24, 25]. In order to reduce the error, the mean values of the slopes are taken as the values of n' and β, and then the values of α can be calculated from eq. (5).

For a given strain rate, activation energy Q can be expressed as:

$$Q = Rn\frac{d\{\ln[\sinh(\alpha\sigma)]\}}{d(1/T)} \tag{8}$$

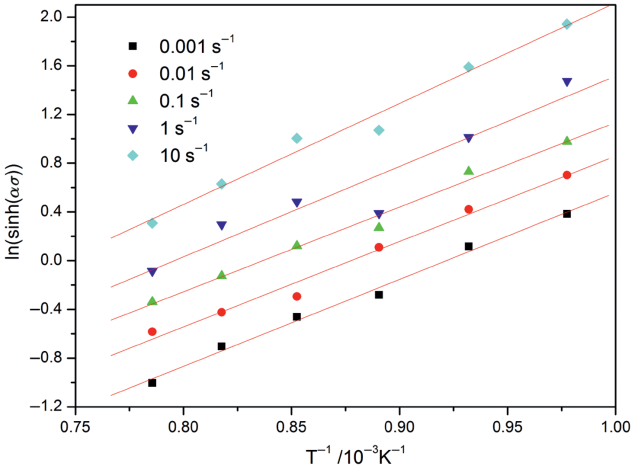

Figure 6: Relationship between ln[sinh(ασ)] and 1/T.

Then the value of Q can be derived from the slopes in the plot of $\ln[\sinh(\alpha\sigma)]$–$1/T$, as illustrated in Figure 6. The value of Q can be obtained to be 425.3 KJ/mol by averaging the Q-values in the strain range of 0.1~0.8 and the interval of 0.1.

Constitutive modeling of flow stress

The evolution of dislocation density is a result of the multiplication and annihilation of dislocations due to WH and DRV respectively and can be expressed as [4]:

$$\frac{d\rho}{d\varepsilon} = U - \Omega\rho \tag{9}$$

where $d\rho/d\varepsilon$ is the increasing rate of dislocation density with strain; U represents the WH (the dislocation storage during the deformation) and can be regarded as constant with respect to strain; $\Omega\rho$ is the contribution of DRV due to dislocation annihilation and rearrangement, and Ω is the coefficient of DRV [17]. When plastic strain $\varepsilon = 0$,

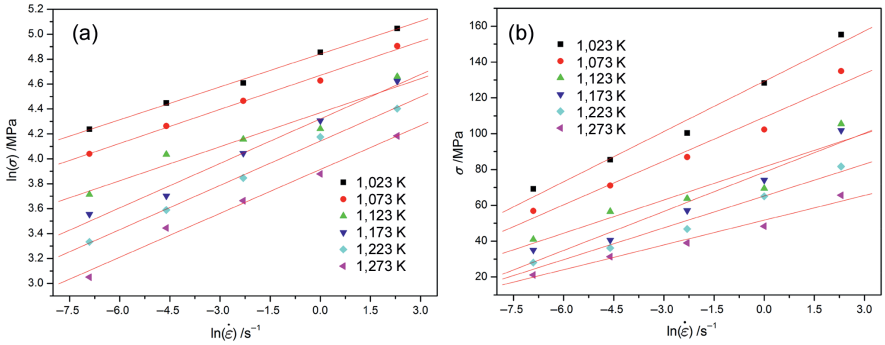

Figure 5: Relationship between: (a) ln(σ) and ln($\dot{\varepsilon}$) (b) σ and ln($\dot{\varepsilon}$).

dislocation density $\rho = \rho_0$, where ρ_0 is the initial dislocation density, and the corresponding flow stress is the initial yield stress σ_0. Then the variations in the dislocation density during the hot deformation can be obtained by integrating eq. (9) as follows:

$$\rho = \rho_0 e^{-\Omega\varepsilon} + \frac{U}{\Omega}(1 - e^{-\Omega\varepsilon}) \tag{10}$$

The contribution of the dislocation density to the flow stress can be expressed as:

$$\sigma = \gamma G d \sqrt{\frac{U}{\Omega}} \tag{11}$$

where γ is Taylor constant, d is the distance between atoms in the slip direction, and G is the shear modulus. Then substituting eq. (11) into eq. (10), the flow stress during the WH and DRV can be represented as:

$$\sigma = [\sigma_{sat}^2 + (\sigma_0^2 - \sigma_{sat}^2)e^{-\Omega\varepsilon}]^{1/2} \tag{12}$$

where σ_{sat} is the saturations tress. The combined effects of temperature and strain rate on feature parameters eq. (12), i. e. σ_{sat}, σ_0 and Ω, can be characterized by the Z parameter (eq. (3)). It is usually assumed that influence of strain on flow stress is insignificant and thereby would not be considered in eq. (12). However, it can be seen from Figure 2 that some stress–strain curves show obvious WH under some deformation conditions (for example, at the temperature of 1,023 K and 1,073 K, strain rate of 1 s^{-1}), then no obvious σ_{sat} can be obtained from the flow stress curves. Therefore, WH should be taken into account in order to derive constitutive equations to predict the flow stress more accurately. The peak stress σ_{peak} is introduced to replace σ_{sat} in eq. (12) for the purpose of improving precision of developed constitutive equation. Meanwhile, it can be found from Figure 3 that the value of σ_{sat} can also be regarded as that of σ_{peak} in the typical DRV curve. Then eq. (12) can be rewritten as:

$$\sigma = [\sigma_{peak}^2 + (\sigma_0^2 - \sigma_{peak}^2)e^{-\Omega\varepsilon}]^{1/2} \tag{13}$$

The values of σ_{peak} under various deformation conditions can be easily obtained from the true stress–strain curves. Figure 7(a) illustrates a linear relation between σ_{peak} and lnZ, then the values of σ_{peak} can be expressed as:

$$\sigma_{peak} = 7.5288 \ln Z - 241.8376 \tag{14}$$

It can be seen from eq. (13) that σ_{peak} has considerable effects on the prediction accuracy of the developed constitutive model. Therefore, the correlation coefficient (R) and the average absolute relative error (*AARE*) between the predicted and measured values are employed to evaluate prediction capability of σ_{peak}. The values of R and *AARE* are 0.9732 and 10.765 %, respectively. In order to further improve prediction accuracy, a third-order polynomial is used to fit the measured values of σ_{peak}, as shown in Figure 7(b) and can be expressed as:

$$\sigma_{peak} = 0.01051(\ln Z)^3 - 1.09119(\ln Z)^2 + 42.69357 \ln Z - 577.95676 \tag{15}$$

The values of R and *AARE* between the third-order polynomial predicted and measured σ_{peak} are 0.9907 and 4.525 %, respectively. Therefore, the expression for the peak stress in the form of the third order polynomial greatly improves its prediction accuracy.

It is difficult to determine the accurate initial yield stress σ_0 by the inflexion points in the actual stress–strain curves. Therefore, the initial yield stress σ_0 at various deformation temperatures and strain rates are taken as the stress corresponding to a strain of 0.02 [1].

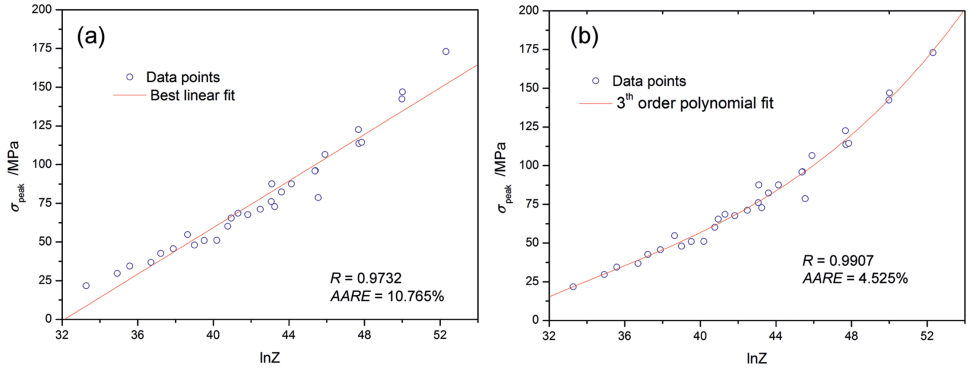

Figure 7: Relationship between σ_{peak} and the lnZ: (a) linear fitting and (b) polynomial fitting.

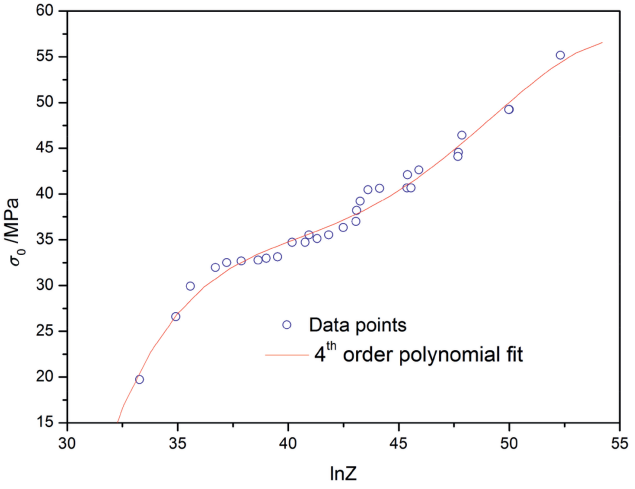

Figure 8: Relationship between the yield stress and the Zener–Hollomon parameter.

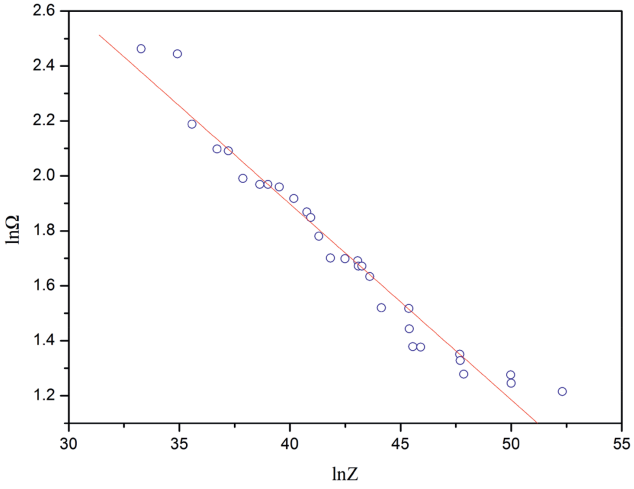

Figure 9: Relationship between Ω and the Zener–Hollomon parameter.

Figure 8 illustrates the relationship between the initial yield stress and lnZ, and a fourth-order polynomial is employed to fit the measured values. Then, the initial yield stress σ_0 can be expressed as:

$$\sigma_0 = -0.000888(\ln Z)^4 + 0.1588(\ln Z)^3 - 10.58476(\ln Z)^2 + 311.95538\ln Z - 3405.98281 \tag{16}$$

According to eq. (13), Ω can be calculated by the following formula:

$$\Omega\varepsilon = \ln\left(\frac{\sigma_{peak}^2 - \sigma_0^2}{\sigma_{peak}^2 - \sigma}\right) \tag{17}$$

Using the true stress–strain data, the values of Ω can be determined for the whole deformation conditions. Figure 9 illustrates that a linear relation exists between lnΩ and lnZ. Meanwhile, it can be found from the figure that lnΩ decreases with the increase of lnZ, and Ω is expressed as a function of Z parameter:

$$\ln\Omega = 4.751 - 0.07132\ln Z \tag{18}$$

Therefore, the physics-based constitutive model of BFe10-1-2 cupronickel alloy during hot working can be summarized as:

$$\begin{cases} \sigma = [\sigma_{peak}^2 + (\sigma_0^2 - \sigma_{peak}^2)e^{-\Omega\varepsilon}]^{1/2} \\ \sigma_{peak} = 0.01051(\ln Z)^3 - 1.09119(\ln Z)^2 + 42.69357\ln Z - 577.95676 \\ \sigma_0 = -0.000888(\ln Z)^4 + 0.1588(\ln Z)^3 - 10.58476(\ln Z)^2 + 311.95538\ln Z - 3405.98281 \\ \ln\Omega = 4.751 - 0.07132\ln Z \\ Z = \dot{\varepsilon}\exp\left(\frac{-425300}{RT}\right) \end{cases} \tag{19}$$

Verification of the developed constitutive equations of BFe10-1-2 cupronickel alloy

In order to verify the developed physics-based constitutive equation, a comparison between the experimental and predicted flow stress data at different strains within the range of 0.15~0.75 and the interval of 0.1 (i. e. the testing data that were not used to fitting curves) was carried out in Figure 10. The predicted flow stress data from the constitutive equation could track the experimental data of BFe10-1-2 cupronickel alloy, and there is a good agreement between the experimental and predicted values under most deformation conditions. Only under some processing condition (i. e. at 1,023 K, 1,173 K in 10 s^{-1} and 1,123 K, 1,273 K in 1 s^{-1}), a remarkable variation between experimental and computed flow stress data could be observed. The main reason of the variation may contribute to the fact that the response of flow behavior of mental materials at evaluated temperatures is highly nonlinear. Most factors affecting the flow stress are nonlinear, which make the accuracy of the predicted flow stress by the constitutive equations low and the applicable range limited [9]. Meanwhile, the fitting of material constants may lead to the variation between experimental and computed flow stress data. For example, experimental data in Figure 5(b) show some deviation. Therefore, some errors may be introduced because of the determination of the values of β and finally affect the accuracy of constitutive equation.

The predictability of the developed physics-based constitutive equation could be quantified in terms of standard statistical parameters such as R and $AARE$. These are expressed as following equations [26]:

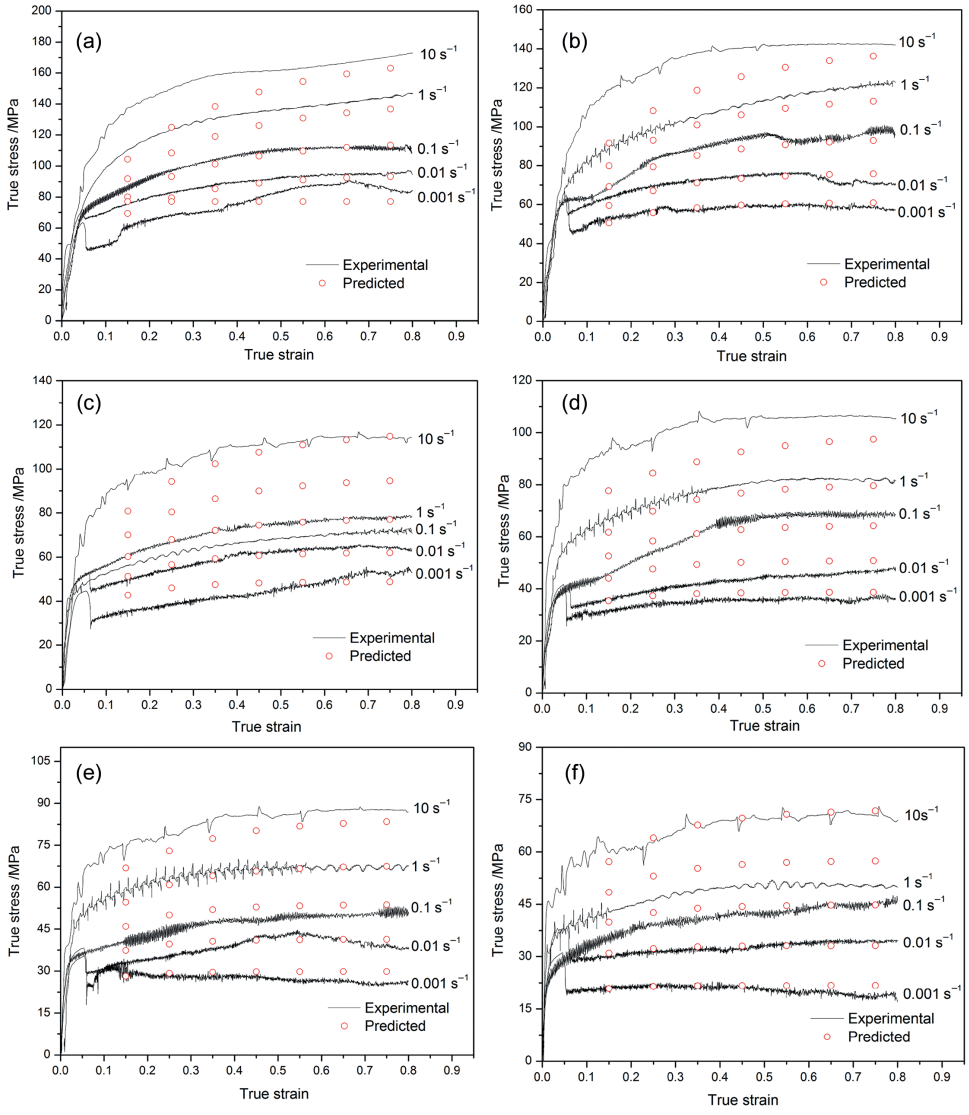

Figure 10: Comparison between the experimental and predicted flow stress at the temperature of: (a) 1,023 K, (b) 1,073 K, (c) 1,123 K, (d) 1,173 K, (e) 1,223 K, (f) 1,273 K.

$$R = \frac{\sum_{i=1}^{N}(E_i - \bar{E})(P_i - \bar{P})}{\sqrt{\sum_{i=1}^{N}(E_i - \bar{E})^2 \sum_{i=1}^{N}(P_i - \bar{P})^2}} \tag{20}$$

$$AARE(\%) = \frac{1}{N}\sum_{i=1}^{N}\left|\frac{E_i - P_i}{E_i}\right| \times 100 \tag{21}$$

where E is the experimental flow stress and P is the predicted flow stress obtained from the developed constitutive equation considering strain compensation. $\bar{E}$ and $\bar{P}$ are the mean values of E and P respectively. N is the total number of data used in this study.

R is a commonly employed statistical parameter and provides information on the strength of the linear relationship between the experimental and predicted data. And the *AARE* is calculated through a term by term comparison of the relative error and therefore is an unbiased statistical parameter for determining the predictability of the equation [27]. As can be seen from Figure 11, although there are some variation under some deformation conditions, the values of R and *AARE* are found to be 0.9833 and 6.726 % respectively, which indicate that the developed physics-based constitutive model gives an accurate and precise estimate of the DRV behavior of BFe10-1-2 cupronickel alloy.

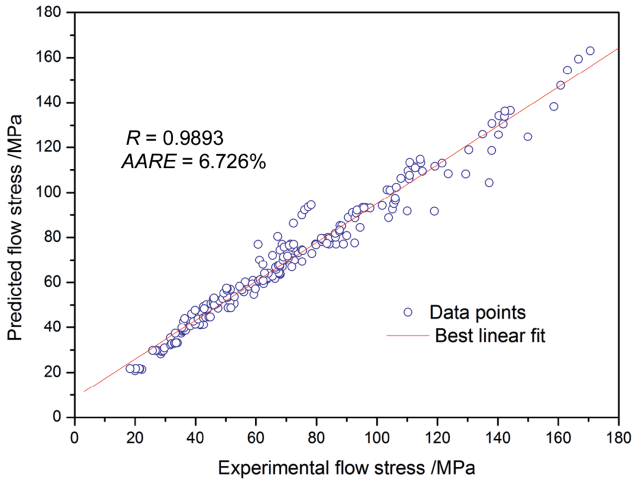

Figure 11: Correlation between the experimental and predicted flow stress data from the developed constitutive equation.

Conclusions

A physics-based constitutive model was developed to describe DRV behavior of BFe10-1-2 cupronickel alloy during hot working by performing hot compression tests over a wide range of temperature (1,023~1,273 K) and strain rate (0.001~10 s^{-1}). Based on this study, following conclusions are obtained:

(1) DRV is the main softening process for BFe10-1-2 cupronickel alloy during hot working.

(2) The developed physics-based constitutive equation can precisely predict the flow stress under most deformation conditions. The predictability of developed constitutive equation was quantified in terms of correlation coefficient (R) and average absolute relative error ($AARE$). The results of R and $AARE$ indicated that the proposed constitutive model could accurately characterize the hot DRV behaviors for BFe10-1-2 cupronickel alloy over a wide range of temperatures and strain rates.

Acknowledgements: The authors gratefully acknowledge the financial support received from Planned Scientific Research Project of Education Department of Shaanxi Provincial Government (15JS056), Innovation Team Project of "Processing and Preparation for High-performance Non-ferrous Metal Materials" of Xi'an University of Architecture and Technology, Fundamental Science Funds of Xi'an University of Architecture and Technology (JC1308) and Talents Science Fund of Xi'an University of Architecture and Technology (RC1369).

References

[1] G.L. Ji, Q. Li and L. Li, Mater. Sci. Eng. A., 615 (2014) 247–254.
[2] J. Luo, M.Q. Li and W.X. Yu, Mater. Des., 31 (2010) 3078–3083.
[3] R.X. Chai, C. Guo and L. Yu, Mater. Sci. Eng. A., 534 (2012) 101–111.
[4] Y.C. Lin and X.M. Chen, Mater. Des., 32 (2011) 1733–1759.
[5] C.M. Sellars and W.J. Mctegart, Acta Metall., 14 (1966) 1136–1138.
[6] Y.C. Lin, M.S. Chen and J. Zhong, Comput. Mater. Sci., 42 (2008) 470–477.
[7] D. Samantaray, S. Mandal and A.K. Bhaduri, Mater. Des., 31 (2010) 981–984.
[8] A.K. Guta, V.K. Anirudh and S.K. Singh, Mater. Des., 43 (2013) 410–418.
[9] H.Y. Li, X.F. Wang, D.D. Wei, J.D. Hu and Y.H. Li, Mater. Sci. Eng. A., 536 (2012) 216–222.
[10] R.S. Yassar, O. Abuomar, E. Hansen and M. Horstemeyer, Mater. Des., 31 (2010) 3683–3689.
[11] Y.C. Zhu, W.D. Zeng, Y. Sun, F. Feng and Y.G. Zhou, Comput. Mater. Sci., 50 (2011) 1785–1790.
[12] X.W. Yang, J.C. Zhu, Z.H. Lai, Y.R. Kong, R.D. Zhao and D. He, Mater. Sci. Technol., 28 (2012) 151–155.
[13] O. Sabokpa, A. Zarei-Hanzaki, H.R. Abedi and N. Haghdadi, Mater. Des., 39 (2012) 390–396.
[14] T. Yan, E.L. Yu and Y.Q. Zhao, Mater. Des., 50 (2013) 574–580.
[15] W. Hu and C.H. Wang, Comput. Mech., 37 (2003) 445–452.
[16] M.A. Mostafaei and M. Kazeminezhad, J. Mater. Eng. Perform., 22 (2013) 700–705.
[17] N.K. Park, J.T. Yeom and Y.S. Na, J. Mater. Process. Technol., 130–131 (2002) 540–545.
[18] W.X. Yu, M.Q. Li and J. Luo, Rare Met., 31 (2012) 7–11.
[19] V. Seetharaman and S.L. Semiatin, Metall. Mater. Trans. A., 33 (2002) 3817–3830.
[20] F. Warchomicka, M. Stockinger and H.P. Degischer, J. Mater. Process. Tech., 177 (2006) 473–477.
[21] S.V. Mehtonen, L.P. Karjalainen and D.A. Porter, Mater. Sci. Eng. A., 607 (2014) 44–52.
[22] S. Mandal, V. Rakesh, P.V. Sivaprasad, S. Venugopal and K.V. Kasiviswanathan, Mater. Sci. Eng. A., 500 (2009) 114–121.
[23] Y.H. Xiao and C. Guo, Mater. Sci. Eng. A., 528 (2011) 5081–5087.
[24] J. Luo, M.Q. Li, H. Li and W.X. Yu, Mater. Sci. Eng. A., 505 (2009) 88–95.
[25] G.L. Ji, F.G. Li, Q.H. Li, H.Q. Li and Z. Li, Mater. Sci. Eng. A., 527 (2010) 1165–1171.
[26] J. Li, F.G. Li, J. Cai, R.T. Wang, Z.W. Yuan and F.M. Xue, Mater. Des., 42 (2012) 369–377.
[27] S. Mandal, P.V. Sivaprasad, S. Venugopal and K.P.N. Murthy, Appl. Soft. Comput. J., 9 (2009) 237–244.